Journal of Alloys and Compounds 509 (2011) 1347–1354

Contents lists available at ScienceDirect

Journal of Alloys and Compounds

journal homepage: www.elsevier.com/locate/jallcom

Structural and magnetic properties of C15 $HoMn_2$ hydrides

A. Budziak[a,*], P. Zachariasz[b], L. Kolwicz-Chodak[c], H. Figiel[c], A. Pacyna[a], J. Żukrowski[c]

[a] The H.Niewodniczański Institute of Nuclear Physics PAN, ul. Radzikowskiego 152, 31-342 Kraków, Poland
[b] Institute of Atomic Energy POLATOM, 05-400 Otwock-Świerk, Poland
[c] Faculty of Physics and Applied Computer Science, University of Science and Technology, Al. Mickiewicza 30, 30-059 Kraków, Poland

ARTICLE INFO

Article history:
Received 14 September 2010
Received in revised form 4 October 2010
Accepted 7 October 2010
Available online 21 October 2010

Keywords:
Laves phase hydrides
Crystal structure
X-ray diffraction
Magnetic measurements
Phase diagram

ABSTRACT

Powder samples of cubic $HoMn_2H_x$ hydrides, with $0 \le x \le 4.3$, have been investigated by X-ray diffraction and AC/DC magnetometry as a function of temperature and external magnetic field. Hydrogen is demonstrated to strongly modify structural and magnetic properties. X-ray studies revealed many structural transformations placed at low temperatures. In particular, a transformation from the cubic to the monoclinic structure was detected, which so far has not been reported for other cubic RMn_2H_x (R – rare earth or Yttrium) compounds. The structural transformations are reflected in the magnetic behavior. The change in ordering temperatures implies a very strong relationship between the magnetic interactions and the Mn–Mn distance modified at hydrogen absorption. Tentative magnetic and structural phase diagrams are proposed. The presented results are compared with the properties of other cubic and hexagonal RMn_2H_x hydrides.

1. Introduction

The hydrides of Laves phase type intermetallic compounds RMn_2 (R – rare earth or Yttrium) have been intensively studied due to their unusual physical properties. These compounds can easily absorb large amounts of hydrogen (about 4.5 H atoms per formula unit). In recent years, many investigations have proved that H atoms usually occupy tetrahedral A2B2 and AB3 sites. In most of the Laves phase hydrides H atoms occupy only A2B2 sites at low hydrogen concentration, whereas AB3 sites start to be filled above $x \sim 3.0$ [1,2]. Significant increase of the relative volume of the unit cell due to hydrogen absorption causes strong modifications of structural and magnetic properties of those hydrides.

Systematic research of the rare earth compounds with Mn shows the important role of Mn–Mn distance, which determines the magnetic interactions in the RMn_2H_x systems and leads to complicated patterns of magnetic ordering. Above the critical value of Mn–Mn distance $d_c \approx 2.7$ Å [3] a strong localization of the magnetic moment at manganese sites is observed leading to a frustrated Mn sublattice [4]. The lattice parameter of our host material $HoMn_2$ $a \approx 7.531$ Å at RT gives Mn–Mn distance ($d_{Mn-Mn} = 2.66$ Å) slightly below the critical value d_c, and therefore after the hydrogenation process we should expect many complex magnetic structures in this system.

The present paper is a next step in a comprehensive work concerning the structural and magnetic properties of RMn_2H_x hydrides (R–Y, Gd, Tb, Dy, Er and Sm).

The pure $HoMn_2$ compound crystallizes either in the cubic C15 or in the hexagonal C14 structure, depending on the heat treatment [5]. Structural and magnetic results presented here were carried out for the C15 structure (space group: *Fd-3m*). We tried to find the similarities to the other RMn_2 cubic structures, simultaneously having in mind a strong affinity of both the C15 and C14 polytypes [6,7]. It is well known, that those structures are closely related to each other, however, it is still unclear whether the difference in cubic or hexagonal packing affects the properties of hydrides.

2. Experimental details

The samples of $HoMn_2H_x$ with different hydrogen concentration $x = 0.55$, 1.0, 1.65, 2.0, 2.5, 3.0, 3.5, and 4.3 were prepared. The standard technique for the sample preparation and hydrogenation process was used as reported elsewhere [8,9]. The quality of the $HoMn_2H_x$ hydrides were checked by X-ray diffraction technique.

The X-ray powder diffraction (XRD) measurements have been carried out on the Siemens D5000 diffractometer with Cu K_α radiation ($\lambda = 1.54056$ Å), and with continuous flow cryostat in the temperature range from 70 to 380 K. The data were collected in a process of heating. At each step the temperature was stabilized (at least 40 min) in order to reach the thermal equilibrium. For identification of the XRD patterns the FullProf program [10] based on the Rietveld method [11] was used.

The AC/DC susceptibility at the temperature range 4–300 K and the field dependence of the magnetization $M(H)$ of the samples were measured with the LakeShore VSM 7225 magnetometer. The temperature dependence of magnetization was obtained using both ZFC and FC modes. The magnetic measurements were done in a process of heating as well.

Additionally, the field dependence of the magnetization $M(H)$ was recorded for hysteresis loops in ±10 kOe field mode using the Lake Shore 7300 magnetometer at 77 K.

* Corresponding author: Tel.: +48 12 662 8142; fax: +48 12 662 8458.
E-mail address: andrzej.budziak@ifj.edu.pl (A. Budziak).

0925-8388/$ – see front matter © 2010 Elsevier B.V. All rights reserved.
doi:10.1016/j.jallcom.2010.10.060

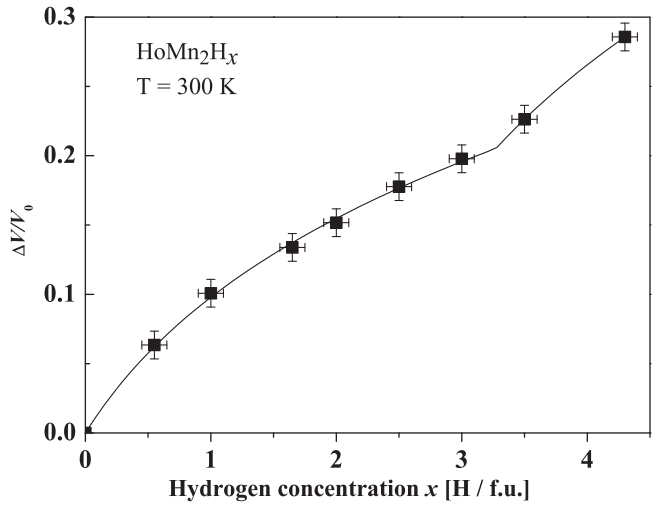

Fig. 1. The relative change of the unit cell volume as a function of hydrogen concentration for $HoMn_2H_x$. The solid line represents the fit to the model from [15].

In the paramagnetic state above the ordering temperature the magnetic behavior was characterized by the Curie–Weiss relation:

$$\chi(T) = \chi_{dia} + \frac{C}{(T - \Theta)} \quad (1)$$

with $\chi_{dia} = -1.6 \times 10^{-7}$ cm^3/g estimated from the tabulated data [12].

3. Results

3.1. The X-ray diffraction results

Most of the $HoMn_2H_x$ (with $x \leq 3.5$) hydrides revealed the single-phase C15 cubic structure at room temperature. Only the sample with $x = 0.55$ consisted of two phases with a different hydrogen content at RT. The disproportion between the H concentrations allows us to suggest the spinodal decomposition of the sample with $x = 0.55$ into hydrogen deficient and hydrogen rich phases. The fully hydrogenated sample with $x = 4.3$ have revealed well-defined rhombohedral structure (space group: $R\bar{3}m$, no. 166). This behavior is very similar to the other cubic systems with Gd, Y and Dy [9,13,14] where that type of structural distortion for saturated hydrides was found.

The increase of hydrogen concentration in the system causes the expansion of the lattice parameters and consequently the growth of the unit cell volume. The relative volume $\Delta V/V_0$ as a function of hydrogen content (Fig. 1) was fitted with Eq. (2) according to the model proposed in [15] yielding parameters: $B_0 = 6 \pm 0.5$, $b = 10 \pm 1$, $X_C = 3.2 \pm 0.1$, $P = 0.6 \pm 0.1$.

$$\begin{cases} \dfrac{\Delta V}{V_0} = \left[\dfrac{B_0 + bx}{B_0}\right]^{1/b} - 1; & \text{for } x < X_C \\ \dfrac{\Delta V}{V_0} = \left[\dfrac{B_0 + b\,(X_C + (1-P)(x - X_C))}{B_0}\right]^{1/b} & \\ \qquad + \left[\dfrac{B_0 + Pb\,((x - X_C))}{B_0}\right]^{1/b} - 2; & \text{for } x \geq X_C \end{cases} \quad (2)$$

The value of the X_C parameter indicates that the filling of AB3 interstitial sites by hydrogen occurs for hydrogen concentrations $x > \sim 3.2$.

The set of lattice parameters gained from diffraction patterns at 70 K and 300 K for all analyzed samples is listed in Table 1. The lattice parameters of rhombohedral and monoclinic structures are converted to the pseudo-cubic system according to the relations: $(a_{rh}{}^* = [2(a_{rh})^2 c_{rh}/(3)^{1/2}]^{1/3}$, $a_m{}^* = [a_m b_m c_m\,(\sin\beta)]^{1/3}$.

3.1.1. The $0 \leq x < 2$ range

In this hydrogen concentration range the sample with $x = 1.0$ reveals the most interesting behavior. The XRD-patterns for this hydride taken at different temperatures are presented in Fig. 2. Two characteristic temperatures of 295 K and 205 K are clearly visible. From the highest temperatures down to 295 K we observe only one cubic structure (the α phase, *Fd-3m* space group) and below this temperature we can see the splitting of it into two structurally different phases. In contrast to other hydrides based on Gd, Tb or Er [9,16,17], only one of them keeps the host structure down to the lowest temperatures. We found that the lattice parameters of this phase are comparable with those of pure $HoMn_2$ (the α_0 phase) compound. However, the other component transforms from the cubic structure to the rhombohedral one (the δ_r phase, $R\bar{3}m$ space group) at 295K and next to the monoclinic one (the ε_r phase, $C2/m$ space group) at ~205 K, which is signaled by a large splitting of the $(2\,2\,0)_{m,r}$ line (Fig. 2). These structural transformations are fully reversible, so heating the sample above the transition point leads to the reconstruction of the uniform cubic structure. These types of transformations were not observed for any RMn_2H_x (*R*: Gd, Y, Dy, Tb, Er, Sm) hydrides [9,13,14,16–18].

More detailed information of the structural transformations for $x = 1.0$ and other samples with $x \leq 1.65$ are presented in Fig. 3. For the sake of clarity and easier comparison, all lattice parameters of the monoclinic and rhombohedral structures are presented as converted to the pseudo-cubic structure (Section 3.1). In the $HoMn_2H_{1.0}$ hydride abundances of the component phases are almost equal at low temperatures with a little advantage of the hydrogen rich phase (Fig. 3d). The δ_r phase is interesting because it can be understood as an intermediate phase between ε_r and α. Its lattice parameters decrease with temperature (range: 200–290 K) and its abundance increases. It can be related to a gradual diffusion of hydrogen from the δ_r to the α_0 phase. Above ~290 K both phases transform to the single α phase.

For $x = 0.55$ two separate phases exist, also structurally different in the whole temperature range (Fig. 3a and b). The lattice parameters of one of them tend again towards those of pure $HoMn_2$ (the α_0 phase) system at lower temperatures (Fig. 3a). For the other phase only one structural transformation at ~200 K is observed, from the monoclinic (ε_r) to the rhombohedral (δ_r) phase which holds to the highest temperatures.

On the basis of the comparison of the lattice parameters of the pure $HoMn_2$ compound and its hydrides with $x = 0.55$ and 1.0 and their relative abundances (Fig. 3a–d) we could calculate the amount of hydrogen in α_0 as ~0.04 H at./f.u. and in ε_r as ~1.6 H at./f.u. The corresponding values are almost identical for both hydrides below ~200 K and comparable with those obtained for (Gd, Tb, Er)Mn_2H_x [9,16,17]. The corresponding abundances of the α_0 and ε_r phases change with the nominal hydrogen concentration of the sample, which is in agreement with the requirement of constant total hydrogen amount in the sample. It is interesting that for the systems with Ho we do not observe the intermediate phase like for hydrides with Tb and Gd but the distortion to lower symmetry for the hydrogen rich phase. We explain the low temperature splitting into two phases, the hydrogen deficient (α_0) and the hydrogen rich (δ_r or ε_r), as being due to the spinodal decomposition, which was already reported for the RMn_2H_x Laves phases [9,16–18] and other RH_x hydrides [19].

For hydride with $x = 1.65$ on cooling a sequence of single-phase transformations ($\alpha \rightarrow \delta_r \rightarrow \varepsilon_r$) is observed like that detected for $x = 0.55$ and 1.0 (Fig. 3e and f). One can see that the temperatures of transformations are insignificantly shifted towards lower temperatures in comparison with those for $x = 1.0$. The lattice parameters do not change monotonically but reveal characteristic jumps which correspond to structural transformations. The comparison of the lattice parameters for $x = 1.65$ with those of hydrogen rich phase

Table 1
Structural parameters of $HoMn_2H_x$ hydrides at 70 and 300 K.

Hydrogen content x	Structure at 70 K	Unit cell parameters [Å]	Structure at 300 K	Unit cell parameters [Å]
0.0	C15	$a = 7.467(6)$	C15	$a = 7.531(3)$
	C15	$a_0 = 7.470(5)$		
		$a_m = 9.376(8)$		$a_0 = 7.645(7)$
0.5		$b_m = 5.532(8)$	2 Phases	$a_r = 7.759(2)$
	C2/m	$c_m = 8.925(0)$	C15	$a^{**} = 7.689(3)$
		$\beta_m = 90.72(0)^\circ$		
		$a_{m,r}{}^* = 7.736(2)$		
	C15	$a_0 = 7.468(3)$		
1.0		$a_m = 9.379(6)$		
		$b_m = 5.537(4)$	C15	$a = 7.776(1)$
	C2/m	$c_m = 8.932(6)$		
		$\beta_m = 90.66(1)^\circ$		
		$a_{m,r}{}^* = 7.738(8)$		
		$a_m = 9.399(6)$		
		$b_m = 5.533(8)$		
1.65	C2/m	$c_m = 8.931(8)$	C15	$a = 7.853(4)$
		$\beta_m = 90.71(1)^\circ$		
		$a_m{}^* = 7.741(2)$		
2.0	C15	$a = 7.879(1)$	C15	$a = 7.894(2)$
		$a_{rh} = 5.633(4)$,		
2.5	$R\bar{3}m$	$c_{rh} = 13.564(4)$	C15	$a = 7.953(7)$
		$a_{rh}{}^* = 7.939(4)$		
	C15	$a = 7.914(7)$		
		$a_{rh} = 5.6562(3)$		
3.0	$R\bar{3}m$	$c_{rh} = 13.761(8)$	C15	$a = 7.998(8)$
		$a_{rh}{}^* = 7.981(6)$		
3.5	C15	$a = 8.045(4)$	C15	$a = 8.061(6)$
		$a_{rh} = 5.829(1)$		$a_{rh} = 5.831(2)$
4.3	$R\bar{3}m$	$c_{rh} = 13.951(1)$	$R\bar{3}m$	$c_{rh} = 13.987(8)$
		$a_{rh}{}^* = 8.180(1)$		$a_{rh}{}^* = 8.189(2)$

$a_m{}^*$, $a_{rh}{}^*$ – parameters of monoclinic and rhombohedral structures converted to pseudo-cubic system, respectively; $a_{0,r}$ – subscripts '0' and 'r' correspond to hydrogen deficient and hydrogen rich phases, respectively; a^{**} – abundance weighted lattice parameter.

for $x = 0.55$ and 1.0 (Fig. 3e) below 205 K shows their mutual overlapping, which confirms the presence of the same monoclinic ε_r structure for all the hydrides. Such reversible transformations could be of martensitic type.

3.1.2. The $2 \le x \le 4.3$ range

The complete temperature dependences of the lattice parameters for $2 \le x \le 4.3$ are presented in Fig. 4. For this x range a combination of two structures, the cubic one (α) and the rhombohedral one (δ) is observed. Lattice parameters of the δ phase were converted to the pseudo-cubic system. Only the sample with $x = 2.0$ persists with the cubic C15 structure in the whole temperature range without any traces of distortion. A small jump of the lattice parameters of the sample is visible at ~295 K.

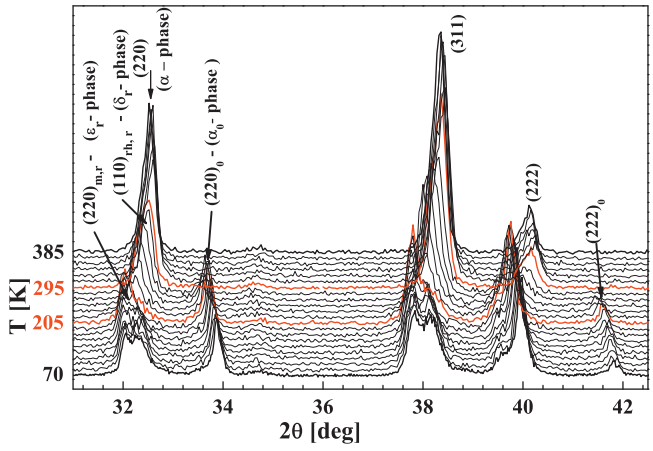

Fig. 2. The temperature evolution of the (2 2 0), (3 1 1) and (2 2 2) diffraction lines for $HoMn_2H_{1.0}$ (see text for more details)..

In contrast, the most complicated behavior is observed for the $x = 2.5$ hydride. From the lowest temperature up to ~305 K a splitting into two phases occurs again. No one of the cubic RMn_2H_x hydrides reveals such a behavior for $2 < x < 3$. Fig. 5 shows the XRD-pattern for $HoMn_2H_{2.5}$ obtained at 70 K with the weighted fit to two structures, cubic α_1 and rhombohedral δ_h. In this case the splitting into two phases is not as obvious as it was for samples with $x = 0.55$ or 1.0. That is why the fit to another monoclinic structure was taken into consideration as well. The Bragg factors for both solutions were comparable, however, the mixture of cubic and rhombohedral structures seems to be more consistent with the final structural phase diagram. For both phases it was possible to estimate the hydrogen contents. The α_1 phase corresponding to lower hydrogen concentration has ~2.3 H at./f.u. and the δ_h phase (higher hydrogen concentration ~2.8 H at./f.u. Abundances of both the phases at 70 K amount to 60% and 40%, respectively. Above the structural transition at ~305 K only one cubic phase (α) is observed. This type of the decomposition into two phases was reported only for hexagonal series (Er, Sm and Nd)Mn_2H_x with $2.0 < x < 3.5$ [17,18,20], which suggests that the cubic $HoMn_2H_x$ hydrides reveal features of hexagonal systems.

The $HoMn_2H_{3.0}$ and $HoMn_2H_{3.5}$ hydrides show the same structural transitions but in different temperature ranges. For sample with $x = 3.0$ the rhombohedral unit cell exists up to 275 K and for $x = 3.5$ up to ~300 K. On further heating both the hydrides undergo a phase transition to the single α cubic phase at ~313 K and ~321 K, respectively, via an intermediate phase ($\alpha + \delta$), see Fig. 4.

For the lattice parameters of the samples with $2.0 \le x \le 3.5$ it was possible to draw a straight line (dotted line, Fig. 4) determining structural transformations or jumps of lattice parameters for these hydrides. It is interesting that thermal expansion coefficients ($(\Delta a/a)/\Delta T$) calculated for the α phase lying to the right of the dotted line are comparable for all the hydrides and amount to $(2.2 \pm 0.1) \times 10^{-4}\,K^{-1}$. The coefficient for the

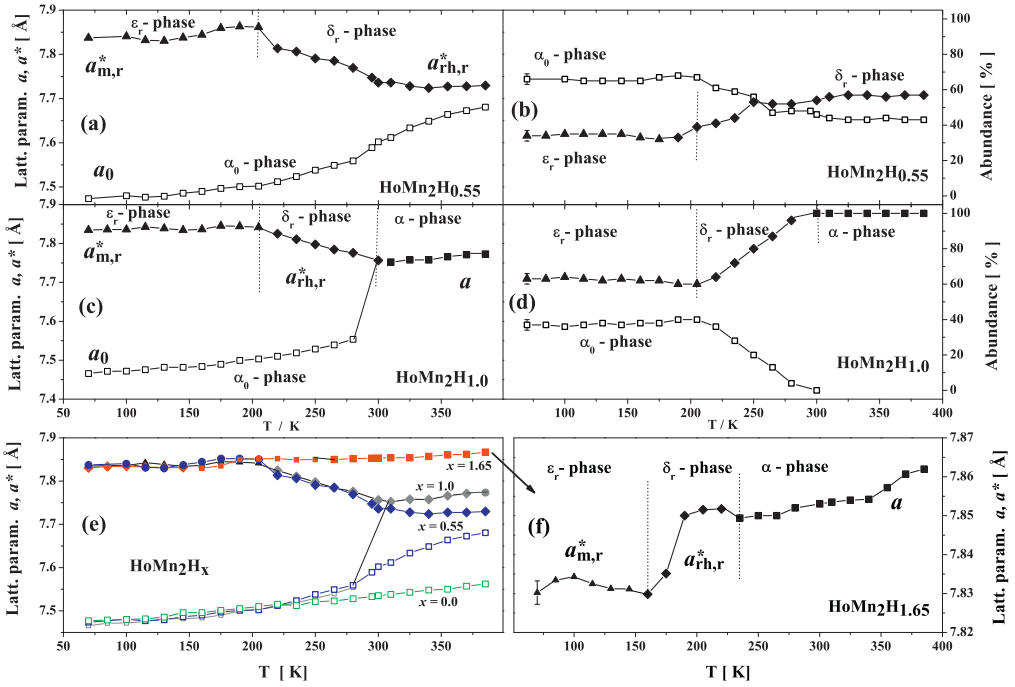

Fig. 3. (a–e) The unit cell parameters and relative abundances of cubic (α, α_0 and α_r), rhombohedral (δ and δ_r) and monoclinic(ε and ε_r) phases for $HoMn_2H_x$ ($x \leq 1.65$) as function of temperature. Descriptions of symbols as in Table 1. If not marked otherwise error bars do not exceed symbol size.

phase with $x = 2.0$ lying to the left of the dotted line reaches $(7.1 \pm 0.1) \times 10^{-5}\,K^{-1}$. It is larger than those of (Tb, Gd)Mn_2H_x $(2.0 < x < 3.0)$ $(\sim 1.0 \times 10^{-5})\,K^{-1}$, which is probably due to Ho behavior in the lattice.

For the sample with hydrogen concentration $x = 4.3$ the single rhombohedral phase δ is observed from the lowest temperatures up to ~365 K (Fig. 6). Above this temperature up to 385 K coexistence of two phases ($\alpha + \delta$) is visible. Further increase of temperature leads to the appearance of the α phase. The process is reversible and decreasing the temperature forces a return to the δ structure. The related behavior (such a high temperature of the first structural transformation) was observed in $GdMn_2H_x$ [9] and it seems to be the result of filling AB3 interstitial sites by hydrogen atoms and it is in agreement with the Hirata–Figiel model [15]. Smaller volume of that type of interstitial site in comparison with A2B2 site could lead to an unstable cubic structure and in consequence the C15 unit cell transforms to the rhombohedral system with lower symmetry but larger volume of the unit cell. However, due to expansion of lattice parameters, above a certain temperature the Westlake's criterion is fulfilled [21] and therefore the system without any restrictions prefers the structure with higher symmetry. It is worth noticing that for $HoMn_2D_{4.5}$ the structural transformation (rhombohedral → cubic) was observed just above RT [22].

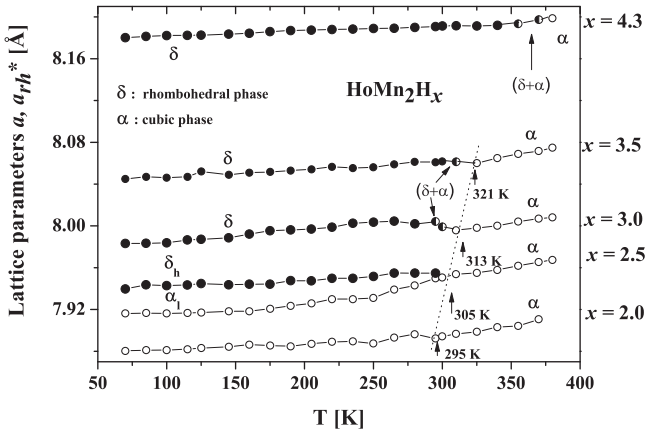

Fig. 4. The lattice parameters and abundances of $HoMn_2H_x$ ($x = 2.0, 2.5, 3.0, 3.5, 4.3$) vs. temperature.

3.2. The magnetic results

The $M(T)$ curves for the various $HoMn_2H_x$ hydrides recorded at the external field of 200 Oe are presented in Fig. 7. The magnetization curves versus external magnetic field $M(H)$ for all the samples and the hysteresis loops for the single-phase hydrides

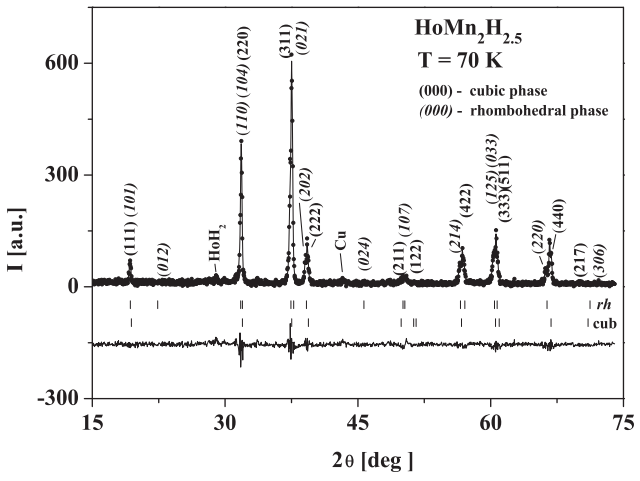

Fig. 5. Observed (symbols), calculated (solid line), and difference (observed-calculated; bottom solid line) X-ray diffraction profiles at 70 K for the $HoMn_2H_{2.5}$ hydride. Upper tick marks indicate the position of the Bragg reflections for the rhombohedral phase, and lower tick marks—for the cubic phase.

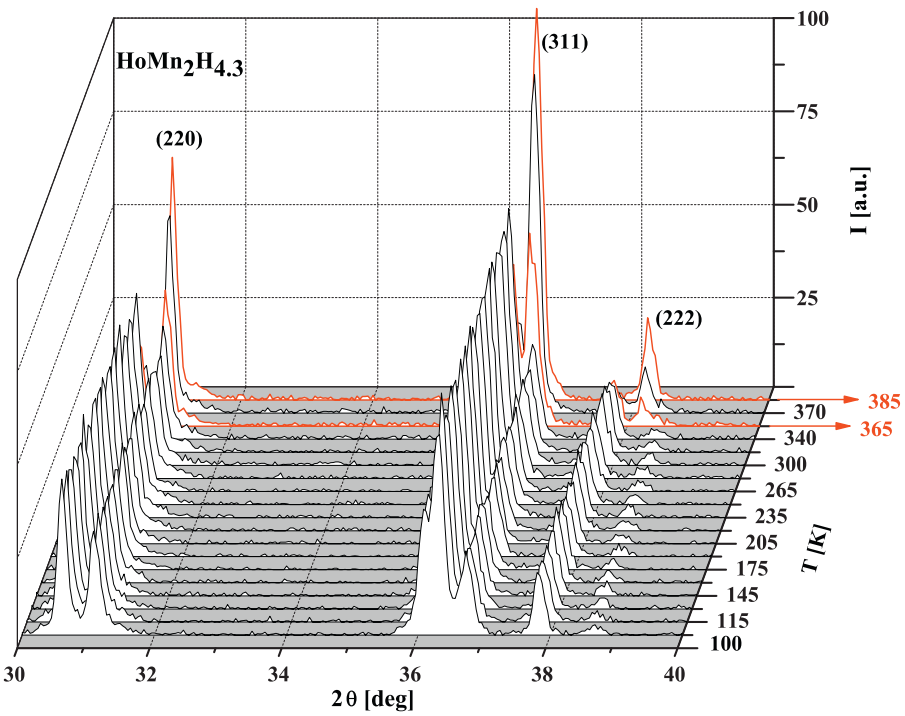

Fig. 6. The temperature evolution of the diffraction lines for $HoMn_2H_{4.3}$. Below 365 K: the δ phase, above 385 K: the α phase. Between 365 K and 385 K: the ($\alpha+\delta$) phases (see text for more details).

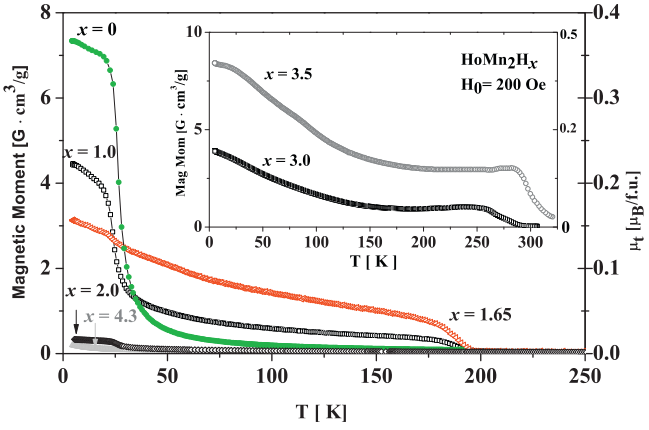

Fig. 7. Weighted magnetic moment of the $HoMn_2H_x$ hydrides versus temperature in the external field of 200 Oe, for various hydrogen concentrations.

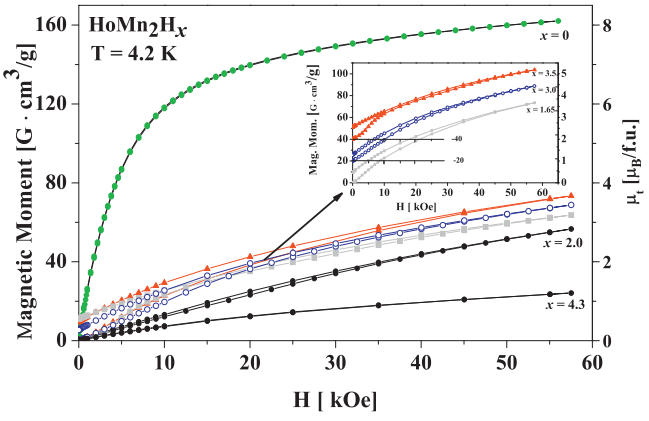

Fig. 8. Magnetization curves vs. external magnetic field for the $HoMn_2H_x$ hydrides at 4.2 K. Insert: Curves for $x = 1.65$, 3.0 are 3.5 are shifted for clarity.

measured at $T = 4.2$ K and 77 K are shown in Figs. 8 and 9, respectively. The magnetic parameters of the samples with $x = 0$, 1.0, 1.65, 2.0, 2.5 as determined for the paramagnetic phase are given in Table 2. For higher concentrations, $x = 3.0$ and 3.5, due to the limit of the experimental range it was only possible to estimate $T_{N,C}$. Table 2 contains magnetic moments (M_{sat}) calculated for the single-phase hydrides and the temperatures of additional magnetic anomalies.

Table 2
Magnetic parameters and characteristic temperatures of the current $HoMn_2H_x$ powder samples.[a]

x [H/f.u.]	μ_{eff} [μ_B/f.u.]	$\theta_{C,N}$ [K]	$T_{N,C}$ [K]	M_{sat} [μ_B/f.u.]	T_M [K]	$T_S \pm 10$ [K]	$T_{SH} \pm 2$ [K]
0.0	10.7 ± 0.1	19.7 ± 0.2	23 ± 1	8.7 ± 0.1	24.3 ± 0.5	–	20
1.0	10.0 ± 0.3	15 ± 10	196 ± 5	–	25 ± 1, 112 ± 1, 188 ± 3	205, 295, 370	200, 215, 230
1.65	9 ± 2	13 ± 20	198 ± 8	–	23 ± 1, 189 ± 3	160, 230	200, 215, 240
2.0	9.0 ± 0.3	−5 ± 3	265 ± 10	6.8 ± 0.2	25 ± 3	295	215, 251, 262
2.5	9 ± 2	30 ± 8	278 ± 8	–	24 ± 2, 29 ± 1, 115 ± 3	305	264, 271
3.0	–	–	306 ± 10	5.6 ± 0.1	30 ± 1, 266 ± 1, 285 ± 1	295, 313	274, 290
3.5	–	–	312 ± 10	5.3 ± 0.4	130 ± 3, 294 ± 2	321	290, 304, 330
4.3	–	–	~(370–375) (expected)	2.7 ± 0.1	–	365, 385	352, 374

[a] μ_{eff}, $\theta_{C,N}$, $T_{N,C}$ – parameters obtained in the paramagnetic state (H = 200 Oe); $\mu_{eff} = (3k_B C_{mol}/N_0(\mu_B)^2)^{1/2}$; M_{sat} – estimated at 4.2 K; T_M – temperatures of additional magnetic anomalies; T_S – temperatures of structural (or volume) transitions obtained by X-ray analysis; T_{SH} – temperatures of peaks of specific heat, underlined – expected temperatures of hydrogen ordering.

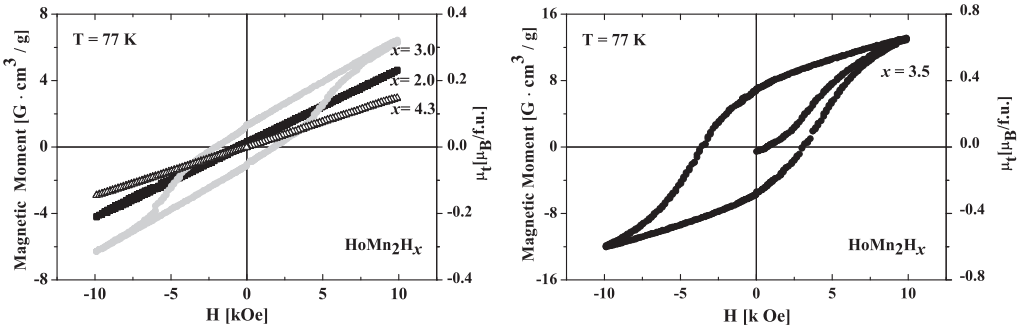

Fig. 9. (a and b) Magnetic moment versus external magnetic field (hysteresis loops) for $HoMn_2H_x$ obtained at 77 K.

3.2.1. *M(H) at 4.2 and 77 K*

Looking at the *M*(*H*) curves at 4.2 K (Fig. 8), it is apparent that no one reaches full saturation even at 56 kOe. $M_{sat} \sim 8.7\ \mu_B$/f.u., obtained for pure $HoMn_2$, is maximal among all the studied samples and is in good agreement with the values reported in [23,24]. In contrast, the smallest value of M_{sat} is revealed by the sample with the maximal hydrogen concentration ($M_{sat} = 2.7\ \mu_B$/f.u. for $x = 4.3$) and the single-phase samples with intermediate *x* values (Table 2). The effective moment of $(10.7 \pm 0.1)\ \mu_B$/f.u. of the $HoMn_2$ compound deduced from the Curie constant can be compared with the individual effective moments of a free Ho^{3+} ion ($10\ \mu_B$) and Mn ions (typically 2.7–4.0 μ_B). As mentioned above the interatomic distance $d_{Mn-Mn} = 2.66$ Å detected at RT for pure $HoMn_2$ is close to the critical distance $d_c = 2.7$ Å and at $T = 4$ K it reaches an even smaller value of $d_{Mn-Mn} = 2.64$ Å. For this distance in RMn_2 it is expected that only 25% of the Mn atoms carry a magnetic moment [25,26]. If we assume a spin-canted structure of $HoMn_2$ argued in [26], then the value of the magnetic moment obtained seems plausible.

The curves of the magnetization versus external magnetic field (±10 kOe) measured at $T = 77$ K for the hydrides with $x = 2.0$, 3.0, 3.5 and 4.3 (Fig. 9) show that the smallest values of magnetization *M*(*H*) reveals again the hydride with a maximal hydrogen content. Flat hysteresis loops for $x = 2.0$ and 4.3 are very similar to those of (Tb, Gd)Mn_2H_x with the same hydrogen concentration, which suggests antiferromagnetic ordering in them.

Much more complicated forms of hysteresis loops are observed for $x = 3.0$ and 3.5 (Fig. 9a and b). Wide hysteresis loops indicate a large magneto-crystalline anisotropy in these samples.

3.2.2. *M(T) for concentrations x ≤ 2.0*

The temperature dependence of *M*/*H* curve for $x = 1.0$ proves the two-phase decomposition of that hydride. Besides the magnetic anomaly at $T_N = 196 \pm 5$ K, which corresponds to a magnetic ordering in the hydrogen rich phase α_r, the second very clear maximum at $T \approx 20$ K appears and is related to T_C of the pure $HoMn_2$ compound. The precise estimation of the magnetic transition temperature gave $T = 24$ K, which is consistent with the previous report [27].

For the hydride with $x = 1.65$ also a magnetic transition was observed. The corresponding transition temperature $T_N = 198 \pm 8$ K falls close to that found for $x = 1.0$, which again indicates that the transition involves the ordering of the hydrogen rich phase α_r. However, in contrast to the $x = 1.0$ hydride, the magnetic susceptibility curve slopes monotonically in the wide temperature range down to ~170 K.

For $x = 2.0$ the estimated magnetic ordering temperature is ~265 K, which is in agreement with a general tendency for increased hydrogen content to raise $T_{N,C}$ and quite well matches the remaining magnetic data given in Table 2. For this concentration the Curie–Weiss theta is negative implying an antiferromagnetic (AF) coupling between the Ho and Mn sublattices. Similarly, for the $TbMn_2D_2$ deuteride having also the host C15 structure in the whole temperature range an AF ordering was found [28].

3.2.3. *Concentrations x ≥ 2.5*

The magnetization vs. temperature curves detected with FC and ZFC modes for the two-phase hydride with $x = 2.5$ are shown in Fig. 10. While the ZFC magnetization has a typical form in the whole temperature range, the FC signal attains zero at $T_{comp} \sim 43$ K, the feature not observed in other RMn_2H_x hydrides. At the compensation temperature the magnetization of the Ho sublattice (M_{Ho}) is equal and pointed in opposite direction to that of the Mn sublattice (M_{Mn}). Below this temperature M_{Ho} exceeds M_{Mn} and above it $M_{Ho} < M_{Mn}$. The contribution M_{Ho} decreases rapidly with increasing temperature, because the coupling between the Ho and Mn sublattice is weak. This effect is similar to that reported for the $R_3Fe_5O_{12}$ garnets which are ferrimagnets [29]. The small bulges on both the curves (Fig. 10) at about 24 K may be related to the similar anomaly detected for the pure $HoMn_2$ compound involving the reorientation effect of the constituent sublattices. Magnetic ordering temperature for the $HoMn_2H_{2.5}$ hydride obtained from the FC magnetization curve was estimated as $T_N = (278 \pm 8)$ K and agrees well with the tendency to increase $T_{N,C}$ with increasing hydrogen concentration.

In contradiction to the rather low magnetization of the $x = 2.5$ hydride huge jumps of magnetizations for the hydrides with $x = 3.0$ and $x = 3.5$ are observed. For both of them either ferrimagnetic or considerably canted antiferromagnetic structures are expected. Such a behavior of magnetization (Fig. 7) motivated us to perform the AC susceptibility measurements. The temperature dependence of the real part of the AC susceptibility χ' for $HoMn_2H_{3.0}$ is depicted

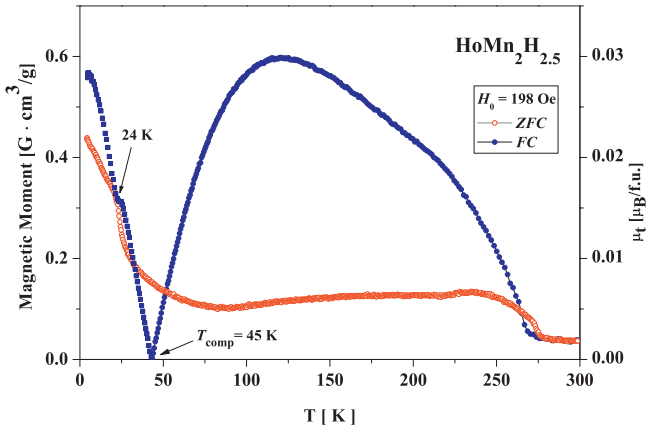

Fig. 10. Temperature dependence of the FC and ZFC weighted magnetic moment for the $HoMn_2H_{2.5}$ hydride in the field of 198 Oe. T_{comp} – compensation temperature (see text).

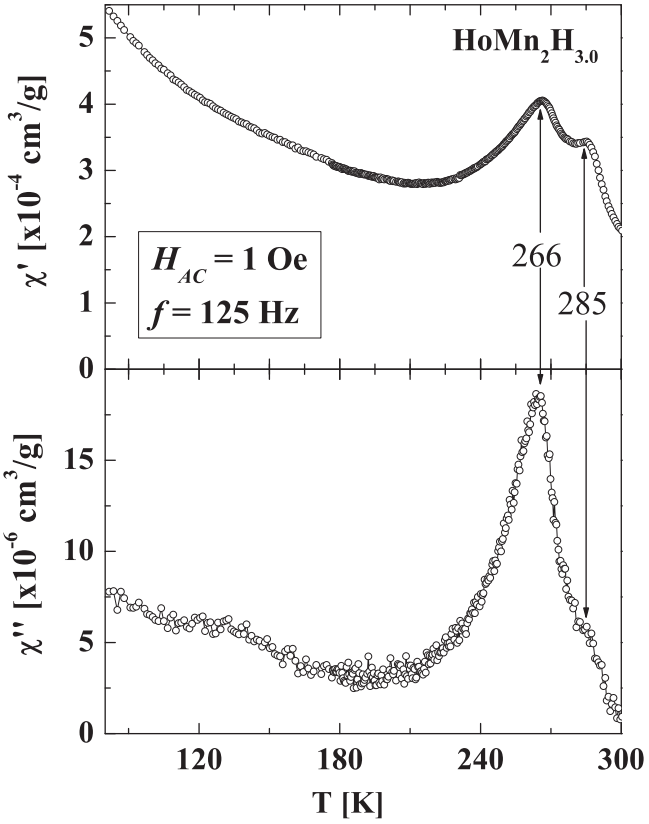

Fig. 11. Temperature dependence of zero-field χ' and χ'' susceptibilities for $HoMn_2H_{3.0}$ with H_{AC} = 1 Oe and f = 125 Hz.

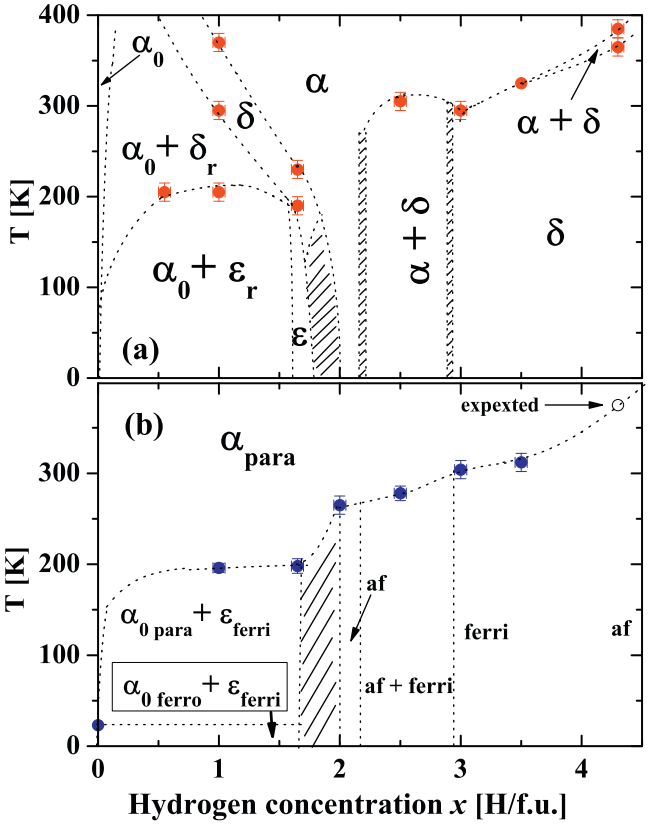

Fig. 12. The proposed phase diagrams for the $HoMn_2H_x$ hydrides: (a) structural; (b) magnetic.

in Fig. 11. Below room temperature, two anomalies at 266 K and 285 K are observed which could be associated with structural transitions: rhombohedral → (cubic + rhombohedral) → cubic at slightly higher temperatures. T_N amounts to (306 ± 10) K and (312 ± 10) K for the x = 3.0 and x = 3.5 hydride, respectively.

For the hydride with the maximal concentration of x = 4.3 a flat magnetization curve $M(T)$ is observed up to RT suggesting purely antiferromagnetic character of the coupling between the Ho and Mn sublattices. On the basis of the XRD measurements one can expect the magnetic ordering temperature above ~370 K, below the structural transition to the cubic phase (~385 K). The antiferromagnetic character of ordering is in agreement with that revealed for $HoMn_2D_{4.5}$ by neutron diffraction [22]. However, transition temperature T_N of the deuteride is almost 100 K lower than that of the hydride and amounts to 280 K. Such a huge difference is very surprising and cannot be explained solely by the replacement of deuterium for hydrogen in these systems.

3.3. Comparison of XRD and magnetic results with specific heat (SH) measurements

The results and discussion of the SH measurements of the $HoMn_2H_x$ are reported in [30]. It is interesting to compare them with the results presented above.

Almost all the SH anomalies observed for the $HoMn_2H_x$ have a peculiar double-peak (or even triple-peak) structure. Only for the $HoMn_2$ sample the phase transition was revealed by a single SH peak at T_N = 20 K, which corresponds very well to the left maximum observed in the temperature dependence of the AC magnetic susceptibility measured along the crystal growth direction [0 0 $\bar{1}$] [23].

The hydrogenation implies a large additional contribution to the specific heat in the whole temperature range of 50–350 K. The increase of hydrogen concentration causes a large increase of the magnetic ordering temperature (e.g. $RMn_2H_{1.0}$, T_N ~ 200 K), which was confirmed above by the magnetic and X-ray measurements. For example, the broad maxima of $C_{mol}(T)$ for the x = 1.0 and 1.65 hydrides between ~170 and 250 K [30] are located in the same temperature range where both the structural (monoclinic → rhombohedral → cubic) and magnetic transformations are observed (Figs. 3–7, Table 2). In this temperature interval, there is an additional peak at ~215 K which is also observed for the single-phase x = 2.0 hydride. In our opinion, it is connected with hydrogen ordering. The more H atoms in a system the more energy (heat) should be invested to order them. That is why the SH values rise with increasing hydrogen concentration. The temperatures at which hydrogen ordering is expected are underlined (T_s column in Table 2 [30]). Also for higher hydrogen concentration, the transformations and characteristic temperatures (especially magnetic ones) are reflected in $C_{mol}(T)$ curves and their maxima. On the basis of the results of the SH measurements for the $HoMn_2H_{4.3}$ sample we can expect magnetic ordering at ~(370–375) K as well.

4. Conclusions

Both structural and magnetic properties of $HoMn_2H_x$ are strongly dependent on hydrogen concentration. On the basis of the X-ray measurements presented above we propose a structural phase diagram shown in Fig. 12a. It can be divided into three separate areas: (1) below x ~ 2.0; (2) above x ~ 2.2, where structural transformations are revealed, and (3) the area where only the single α phase is observed.

In area (1) for $x < \sim 1.6$, the spinodal decomposition into the hydrogen deficient α_0 ($x \sim 0.04$) and hydrogen rich ε_r ($x \sim 1.6$) phases is observed at the lowest temperatures. The α_0 phase corresponds to the cubic phase of the host material, however, the α_r one is the monoclinic structure which transforms to the rhombohedral phase (ε_r) above ~200 K. At higher temperatures, depending on the hydrogen concentration, the α_0 and ε_r phases coexist ($x < \sim 0.5$) to the highest temperatures or, for $\sim 0.5 < x < \sim 1.6$, transform to the single δ phase to finally reach the original α phase. In this area there are no intermediate phases which were typical for (Gd, Tb)Mn_2H_x hydrides [9,16]. No spinodal decomposition was detected for the hydride with $x = 1.65$. What was observed is only the transformations $\varepsilon \rightarrow \delta \rightarrow \alpha$ between single phases at ~230 K and ~250 K, respectively. For higher hydrogen concentration, just below $x \sim 2.0$, a multiphase state is expected (dashed area).

In area (2), for $\sim 2.2 < x < \sim 2.8$, the spinodal decomposition was also observed. Two phases, α and δ, exist from the lowest temperature up to RT without any trace of the monoclinic phase. Such a behavior is known to be typical for hexagonal (Er, Sm)Mn_2H_x hydrides [17,18]. For $x > \sim 2.8$, starting from the lowest temperatures up to ~300–365 K, the single phase δ is observed, followed by the transformation to the cubic α phase above ~300–400 K either directly (for $\sim 2.8 < x < \sim 3.5$) or via an intermediate two-phase ($\alpha + \delta$) area (for $x > \sim 3.5$). Almost an identical transformation to the cubic phase above 400 K was reported for the cubic $GdMn_2H_{4.3}$ hydride [9].

The expansion rates are small and comparable with those observed for the YMn_2H_x hydrides, which indicates substantial damping of spin fluctuations.

The structural transformations are reflected in the magnetic phase diagram (Fig. 12b). For $x = 1.0$ the temperatures of structural transformations T_S exceed the magnetic ordering temperature $T_{N,C}$. The first structural transformation $\varepsilon_r \rightarrow \delta_r$ is close to the magnetic transition detected at ~196 K. For $x = 1.65$ no correlation between the magnetic and structural transformations is apparent. By contrast, in the range $\sim 2.0 < x < \sim 3.5$ involving the α and/or δ phases, the samples order magnetically at T_N ranging from ~265 K up to ~312 K. For $x > \sim 3.5$ a further increase of the magnetic ordering temperature is expected with ~375 K predicted for the maximal hydrogen concentration. The steady increase of the magnetic ordering temperature with increasing hydrogen concentration was also observed for (Gd, Y, Tb)Mn_2H_x [9,13,16]. Such a correlation indicates that the magnetic transitions are predominantly determined by the magnetic interactions within the Mn sublattice. Increase of the Mn–Mn distance, much above the critical distance d_c, leads to a better localization of the Mn magnetic moments and as a result to a substantial increase of the ordering temperatures of the hydrides.

References

[1] A. Somenkov, A.V. Irodova, J. Less-Common Met. 101 (1984) 481.
[2] K.P. Yvon, P. Fisher, in: L. Schlapbach (Ed.), Hydrogen in Intermetallic Compounds I, Springer, Berlin, 1988.
[3] H. Wada, H. Nakamura, K. Yoshimura, M. Shiga, Y. Nakamura, J. Magn. Magn. Mater. 70 (1987) 134.
[4] M.D. Nunez Regueiro, C. Lacroix, J. Magn. Magn. Mater. 140–144 (1995) 1753.
[5] K. Inoue, H. Imai, J. Phys. Soc. Jpn. 66 (1997) 224.
[6] R.L. Berry, G.V. Raynor, Acta Cryst. 6 (1953) 178.
[7] R.L. Johnston, R. Hoffmann, Z. Anorg. Allg. Chem. 616 (1992) 105.
[8] J. Żukrowski, M. Strecker, G. Wortmann, J. Przewoźnik, K. Krop, J. Alloys Comp. 261 (1997) 47.
[9] J. Żukrowski, H. Figiel, A. Budziak, P. Zachariasz, G. Fisher, E. Dormann, J. Magn. Magn. Mater. 238 (2002) 129.
[10] J. Rodrigues-Carvajal, Full Prof ver.2.5, ILL, 1994 (unpublished).
[11] M.H. Rietveld, J. Appl. Cryst. 2 (1969) 65.
[12] P.W. Sellwood, Magnetochemistry, Interscience, New York, 1956, p. 78.
[13] H. Figiel, J. Przewoźnik, V. Paul-Boncour, A. Lindbaum, E. Gratz, M. Latroche, J. Alloys Comp. 274 (1998) 29.
[14] J. Przewoźnik, J. Żukrowski, K. Freindl, E. Japa, K. Krop, J. Alloys Comp. 284 (1999) 31.
[15] H. Figiel, S. Osuchowski, A. Paja, Phys. Stat. Sol. A 204 (10) (2007) 3286.
[16] H. Figiel, A. Budziak, J. Żukrowski, G. Fisher, M.T. Kelemen, E. Dormann, J. Alloys Comp. 335 (2002) 48.
[17] H. Figiel, A. Budziak, P. Zachariasz, J. Żukrowski, G. Fisher, E. Dormann, J. Alloys Comp. 368 (2004) 260.
[18] H. Figiel, A. Budziak, J. Żukrowski, Solid State Commun. 111 (1999) 519–524.
[19] Fukai, The Metal—Hydrogen System, Springer Series in Materials Science No. 21, Springer Verlag, 1993.
[20] A. Budziak et al, not published.
[21] D.G. Westlake, J. Less-Common Met. 91 (1983) 1.
[22] I.N. Goncharenko, I. Mirebeau, A.V. Irodowa, E. Suard, Phys. Rev. B 59 (1999) 9324.
[23] E. Talik, M. Kulpa, A. Winiarski, T. Mydlarz, M. Neumann, J. Alloys Comp. 316 (2001) 51–57.
[24] K. Hardman, J.J. Rhyne, S. Malik, W.E. Wallace, J. Appl. Phys. 53 (3) (1982) 1944.
[25] C. Ritter, S.H. Kilcoyne, R. Cywinski, J. Phys. Condens. Matter 2 (1912) 727.
[26] C. Ritter, R. Cywiński, S.H. Kilcoyne, S. Mondal, J. Phys. Condens. Matter 4 (1992) 1559.
[27] Y. Makihara, Y. Andoh, Y. Hashimoto, H. Fujii, M. Hasuo, T. Okamoto, J. Phys. Soc. Jpn. 52 (1983) 629.
[28] A. Budziak, H. Figiel, J. Żukrowski, E. Gratz, B. Ouladdiaf, J. Phys. Condens. Matter 13 (2001) L871.
[29] S. Geller, J.P. Remeika, R.C. Sherwood, H.J. Williams, G.P. Espinosa, Phys. Rev. 137 (1965) 1034.
[30] Z. Tarnawski, L. Kolwicz-Chodak, H. Figiel, N.T.H. Kim-Ngan, A. Kozłowski, T. Dawid, L. Havelac, K. Miliyanchuk, E. Santava, J. Alloys Comp. 446–447 (2007) 415–418.